Traveling-Wave Masers for Radio Astronomy in the Frequency Range 20–40 GHz

ERIK L. KOLLBERG AND P. THOMAS LEWIN

Abstract—**Tunable rutile traveling-wave masers (TWM's) have been developed for the frequency ranges 20–25 GHz and 29–35 GHz. Operating data for iron-doped rutile are given and the optimum concentration of iron has been determined. A new type of dielectric image line slow-wave structure (SWS), particularly useful in the frequency range 10–50 GHz, is used in two of the masers. This SWS is found superior to the other structure tested, the dielectrically loaded waveguide. For both types of masers, a ferromagnetic isolator is used in order to ensure the gain stability of better than ±0.2 dB at 30 dB net gain, required for radio astronomical applications. The instantaneous 3-dB bandwidth is 30–60 MHz, depending on the maser. The maser package noise temperature at the input waveguide flange was measured to 27 ± 4 K.**

I. Introduction

In radio astronomy, the requirement of the maximum possible sensitivity means that maser amplifiers often are the best choice, since they offer, in practice, the lowest possible noise temperature. Masers usually have moderate bandwidths (5–50 MHz) and are therefore used mainly in spectral line work [1]. In practice, masers have until now been built from 1 up to about 40 GHz [2]–[6]. The higher the frequency the better the noise properties of the maser become, compared with those of any other amplifier, e.g., the parametric amplifier [7].

In the design of a traveling-wave maser (TWM), the maser crystal and the circuit which couples the signal wave to the crystal are the most demanding tasks. For maser crystals, one has until now mainly used ruby (Cr^{3+} in Al_2O_3) and chromium or iron-doped rutile in practical TWM's. There is an advantage of rutile over ruby at higher signal frequencies, due to a larger zero field splitting and stronger mixing of spin states. This means that for rutile, at the high magnetic fields necessary for high signal frequencies, almost any transition has a fair intensity, while for ruby the pure spin states obtained at high fields cause great difficulties in pumping the masers. The highest frequency for which maser action has been demonstrated is for rutile 90 GHz [8] and for ruby 35 GHz [4].

The type of slow-wave structure (SWS) used as the interaction circuit of a TWM has to be tailored to the particular maser crystal considered. Rutile, used in the masers described below, has a dielectric constant of 120 perpendicular and 240 parallel to the optic axis of the crystal. Pure dielectric slowing will consequently give a slowing factor of $\sqrt{120}$ [see (1)]. The high dielectric constant also means that the mechanical tolerance problem becomes more severe, as the signal wavelength in rutile, $\lambda_0/\sqrt{\varepsilon_r}$, is decreased at short wavelengths. It is therefore almost impossible to use transverse-tape arrays such as the comb-line filter type [9] and other solutions have to be found. We will describe two types of SWS's suitable for rutile. One of the structures in particular is mechanically simple and rugged enough to allow construction of masers up to about 50 GHz. The masers described have been developed for the new 66-ft millimeter-wave radio telescope at the Onsala Space Observatory, south of Göteborg, Sweden.

Manuscript received February 16, 1976; revised May 12, 1976. This work was supported by the Swedish Board for Technical Development.

The authors are with the Research Laboratory of Electronics and the Onsala Space Observatory, Chalmers University of Technology, Göteborg, Sweden.

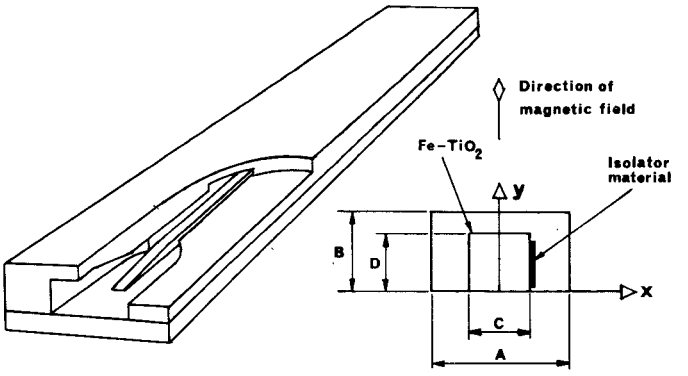

Fig. 1. Exploded view and cross-sectional dimensions of the masers. For the dielectrically loaded waveguide maser $D = B$.

II. The Traveling-Wave Masers

Iron-doped rutile (TiO_2) was used as the maser material in two different types of SWS's; the dielectrically loaded waveguide and the dielectric image line (see Fig. 1). As will be shown, the dielectric image line is superior to the waveguide-type SWS, since more gain for the same crystal length is available and it is more easily manufactured for higher frequencies.

Three masers were manufactured and tested, one waveguide maser for 20–25 GHz and two dielectric image line masers for 22–24.5 GHz and 29–35 GHz. The masers are operated at a liquid helium temperature of 2 K (a helium gas pressure of 30 torr). Gain data for these three masers are given in Fig. 2. The instantaneous 3-dB bandwidth is 25 MHz for the waveguide maser and 60 MHz for the 22-GHz dielectric image line maser. The 35-GHz maser has, at present, a 30-MHz bandwidth, but it should be capable of a 60-MHz bandwidth when more pump power becomes available. It should also be mentioned that the 22-GHz dielectric image line maser is a first prototype design. It should be possible to achieve the same relative tunable bandwidth as obtained for the 30-GHz maser, i.e., 20 percent, by using the same relative dimensions.

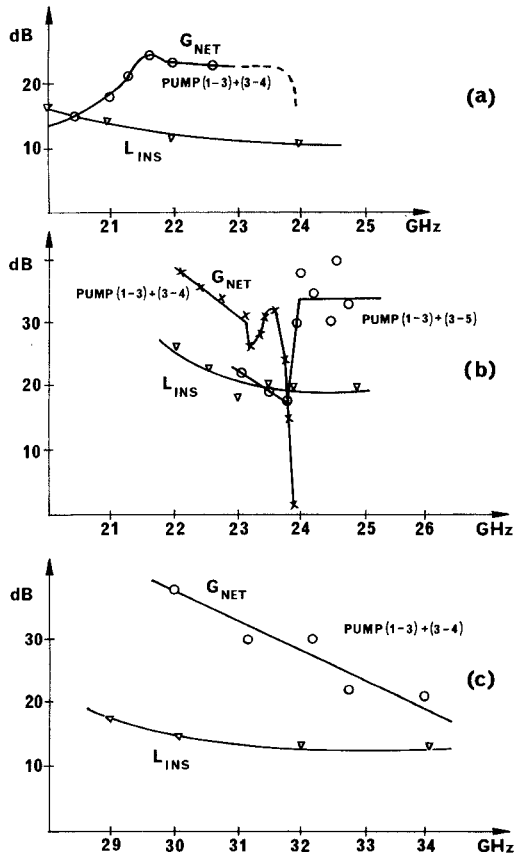

Fig. 2. Net gain and SWS insertion loss of (a) the 22-GHz waveguide maser, (b) the 22-GHz image line maser, and (c) the 30-GHz image line maser.

The various design criteria of the TWM's can conveniently be discussed using the net-gain formula (see, e.g., [9]).

$$G = 27.3 \cdot \frac{LS}{\lambda_0}\left(\frac{1}{Q_m} - \frac{1}{Q_0}\right) \quad \text{(dB)} \tag{1}$$

where L is the physical length of the SWS, S is the slowing factor (equal to the ratio between the velocity of light in vacuum and the group velocity of the signal wave), Q_m is the magnetic quality factor of the maser crystal, and Q_0 is the quality factor representing the signal loss in the SWS. The first term of (1) ($\sim 1/Q_m$) is referred to as the electronic gain (G_{el}) and the second term represents the insertion loss (L_{ins}).

III. The Maser Crystal

The masers described in this paper use iron-doped rutile as the active material, operated with the dc magnetic field along the a axis of the rutile. The 1–2 transition is used as the signal transition. The magnetic quality factor [(1)] is given by [9]

$$1/Q_m = 1.3 \cdot 10^{-18}\,\frac{(-I)\cdot N \cdot \Delta n_0}{\Delta f_l} \cdot \frac{\int_{\text{crystal}} \bar{H}^*\bar{\sigma}\bar{\sigma}^*\bar{H}\,dv}{\int_{\text{structure}} \bar{H}^*\bar{H}\,dv} \tag{2}$$

where N is the number of paramagnetic ions per m^3, $N \cdot \Delta n_0 = N_{10} - N_{20}$ is the population difference in m^{-3}

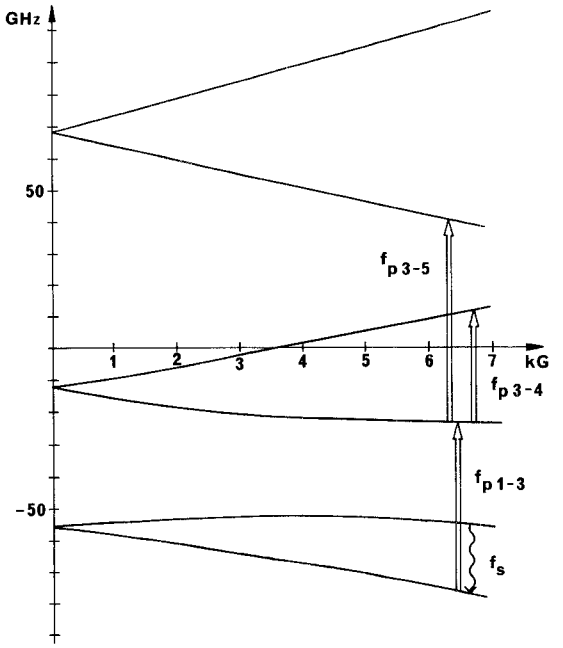

Fig. 3. Pumping schemes for the a-axis operating point.

for the two signal levels when at thermal equilibrium, and $-I(N_{10} - N_{20}) = N_2 - N_1$ is the inverted population difference obtained when the maser crystal is pumped by an external source. I is referred to as the inversion ratio, Δf_l is the linewidth assuming a Lorentzian line shape, $\bar{H}$ is the RF magnetic field, and $\bar{\sigma}$, which is a dimensionless vector, determines the interaction intensity and is a property of the maser crystal only (see [9]). In general, it is possible to get a larger value for $\bar{H}^*\bar{\sigma}\bar{\sigma}^*\bar{H}$ with a dopant having $S = 5/2$ than with one having $S = 3/2$. The quantity $\bar{H}^*\bar{\sigma}\bar{\sigma}^*\bar{H}/\bar{H}^*\bar{H} = |\sigma|^2$ is, of course, determined by the maser crystal ($\bar{\sigma}$) and by the SWS ($\bar{H}$) and is always less than 4.5 ($S = 5/2$) and 2 ($S = 3/2$), respectively, with an equality occurring for pure spin states and circularly polarized fields [9]. Since Fe^{3+} has $S = 5/2$ and Cr^{3+} has $S = 3/2$, there is a potential advantage of iron-doped over chromium-doped crystals. At the a-axis operating point of rutile, the quantity $|\bar{\sigma}|^2 \approx 3.5$ at 22 GHz in the actual SWS.

Two pump sources (klystrons) are used for inverting this crystal. One may alternatively pump the (1–3) + (3–4) or (1–3) + (3–5) transitions (see Fig. 3). In Fig. 4 we have depicted the transition frequencies versus the dc magnetic field. It is noteworthy that there are several crossings between various transitions, where cross relaxation [9] will occur. Hence at 6.25 kG the (2–3) and (4–5) transitions will cross-relax and therefore tend to get the same "temperature." Thus the 2–3 transition is cooled, which means that N_2 has to increase while $N_1 = N_3 = N_4$. This phenomenon is observed as an increase in gain around 21.7 GHz, as seen in Fig. 2(a). At 7.3 kG the (1–2) and (4–5) transitions cross, causing a sharp decrease in gain at 23.9 GHz as shown in Fig. 2(b). However, pumping (1–3) + (3–5) means that the (4–5) transition may also invert and give sufficient gain as seen in Fig. 2(b). By inspecting Fig. 4

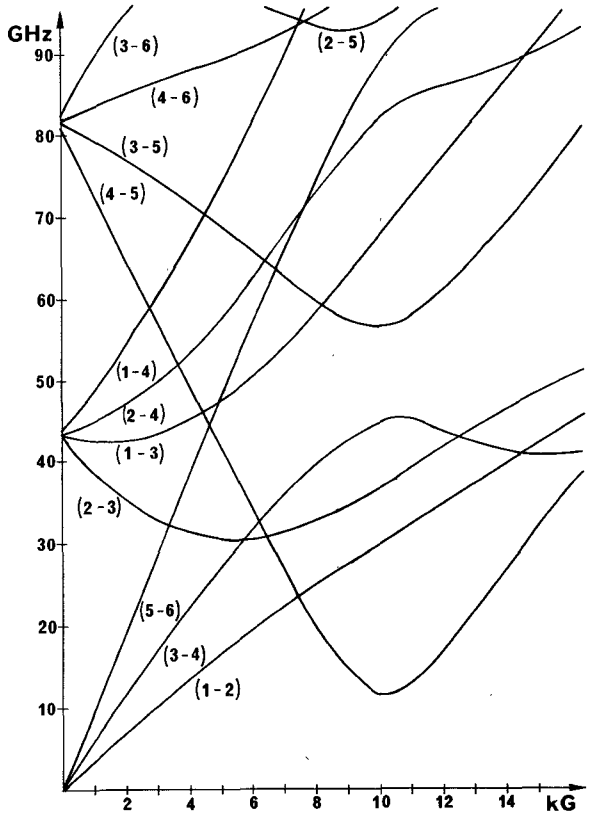

Fig. 4. Transition frequencies versus applied magnetic field for the a-axis operating point. The circles indicate points where cross relaxation has been observed.

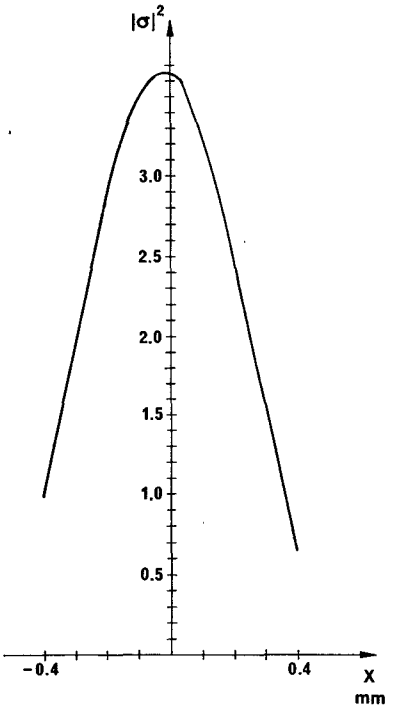

Fig. 5. The interaction intensity $|\bar{\sigma}|^2$ versus x for the dielectric image line as obtained from the approximate theory of Section V.

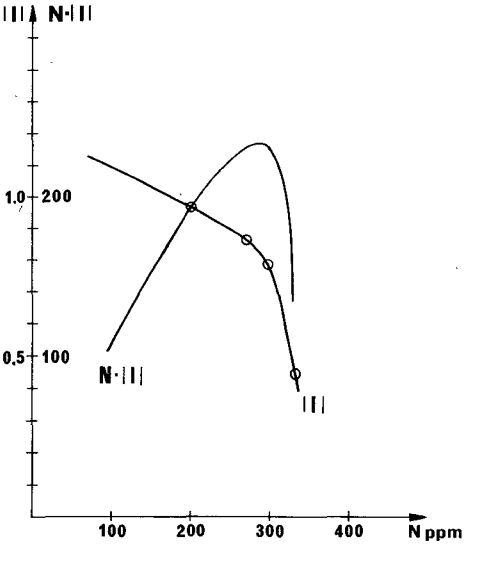

Fig. 6. Measured inversion ratios (I) and dopant concentration times inversion ratio ($N \cdot I$) versus concentration.

it is also seen that there are several similar crossings around 42 GHz. The influence of these crossings are not so easily determined theoretically and have to be determined by future experiments.

The inversion ratio and the linewidth Δf_l are both functions of the dopant concentration N. However, Δf_l is to a greater extent determined by inhomogeneities of the magnetic field, deliberately created and/or due to a magnetic-field perturbation caused by the isolating ferromagnetic material, deposited at the side of the crystal (see Fig. 1). In the present masers, the broadening due to the isolator is dominating. For an estimation of the magnetic-field perturbation on the linewidth, one has to know how much various parts of the crystal contribute to the amplification process, i.e., $\bar{H}^* \bar{\sigma} \bar{\sigma}^* \bar{H}$ has to be considered. For the particular masers described in this paper, a typical plot of $\bar{H}^* \bar{\sigma} \bar{\sigma}^* \bar{H}$ versus x (see Fig. 1) is shown in Fig. 5. Notice the pronounced maximum in the middle of the crystal, which is favorable for keeping the broadening at a low value. The form of $\bar{H}^* \bar{\sigma} \bar{\sigma}^* \bar{H}$ also indicates that the backward wave gain will be almost as large as the forward wave gain, which increases the requirements on the isolation.

Since Δf_l consequently is only weakly dependent on N_1, maximum gain is obtained when the product $-I \cdot N$ is maximum. Experiments at 22 GHz (see Fig. 6), indicate that there is a broad maximum around $N = 1 \cdot 10^{25}$ m^{-3} which corresponds to a dopant concentration of 0.026 percent by weight. The corresponding inversion ratio is $I = -0.85$. Now, comparing our result with results obtained for ruby, where $I = -1.8$, $|\sigma|^2 \approx 1.2$ and $N = 2 \cdot 10^{25}$ [6], one may draw the conclusion that ruby is superior to rutile (we may assume that the linewidth is the same, if it is determined by the isolator). However, since ruby has a dielectric constant of 10, the SWS's used in a ruby and a rutile TWM are quite different. The maser has to be looked upon as a complete device: maser crystal plus slow-wave circuit.

It should be mentioned that most of the maser crystals used in our experiments have been prepared from undoped boules of rutile.[1] The pure rutile was cut in a shape roughly as required for the maser. Thereafter iron was evaporated on a surface perpendicular to the c axis, the easy direction for diffusion of iron. The diffusion was performed at 1200°C for about 24 h in oxygen gas that had passed through water. The added water vapor is essential to avoid creation of lattice faults during the doping process. During the last few hours at 1200°C, and during the cooling down, the water vapor is removed from the gas by letting the gas pass through a drying arrangement with silica gel, ascarite, dehydrite, and finally sicapent as absorbing agents. Then most of the H^+ interstitials, to a great extent located at the Fe^{3+} ions, disappear and only one strong EPR spectrum is obtained [10]. When the doping procedure is finished, the crystal is polished down to its final dimensions.

IV. The Dielectrically Loaded Waveguide Maser

This maser is essentially similar to the one described by Arams and Peyton [5]. One main advantage of this maser is the mechanical simplicity as compared to resonant structures such as a comb structure [3], [4]. It can also be easily isolated as described in the following. Since the relative dielectric constant of rutile is as high as 120 along the a axis and 240 along the c axis, small gaps between the maser crystal and the waveguide walls considerably affect the properties of the SWS. In order to solve the fitting problem, a soft metal folium (gold) was used. The metallic waveguide was made from titanium, which has almost the same coefficient of thermal expansion as rutile. Still, it was virtually impossible to avoid breaking the crystal when the maser was assembled and repeatedly cooled.

In the present masers, the crystal was oriented in such a way that the a axis was parallel to the RF electric field (Fig. 1). Therefore, the properties of the structure could be calculated exactly [11] assuming an isotropic relative dielectric constant ε_r equal to 120. Hence, the $\omega - k$ diagram is determined from

$$\sqrt{k^2 - \omega^2/c_0^2}\ \text{cotanh}\left[\sqrt{k^2 - \omega^2/c_0^2}\cdot(A - C)/2\right] = \sqrt{\varepsilon_r\omega^2/c_0^2 - k^2}\ \tan\left[\sqrt{\varepsilon_r\omega^2/c_0^2 - k^2}\cdot C/2\right]. \quad (3)$$

Also, the RF fields may be calculated exactly. Therefore, everything except for the line shape (or linewidth) in (1) and (2) can now be calculated. In Fig. 7 the $\omega - k$ diagram of a waveguide maser is depicted. In Fig. 8 design data for the 22-GHz maser are shown. In the design one has to find a suitable compromise between electronic gain (G_{el}), isolation (L_B), and the forward wave attenuation in the isolator (L_F). The absolute scales for the gain and isolator attenuations have to be determined experimentally. In Table I we have listed the cross-sectional dimensions of the waveguide maser described in Fig. 1 ($B = D$).

[1] Purchased from Hrand Djevahirdjian, Montey, Switzerland.

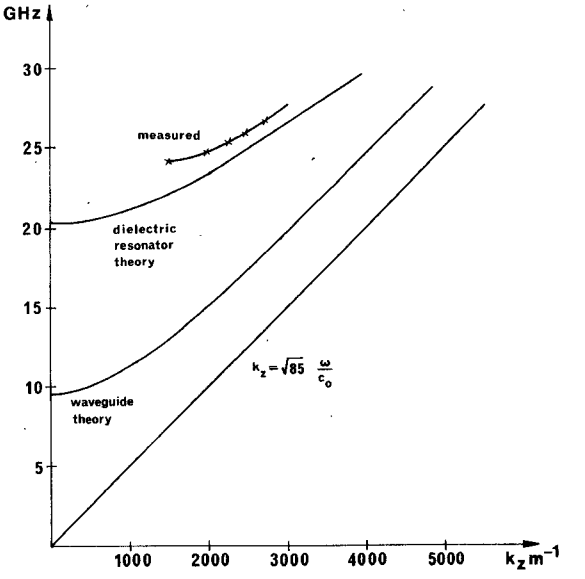

Fig. 7. Dispersion curves for the fundamental mode and the two lowest order higher modes of the dielectric image line maser.

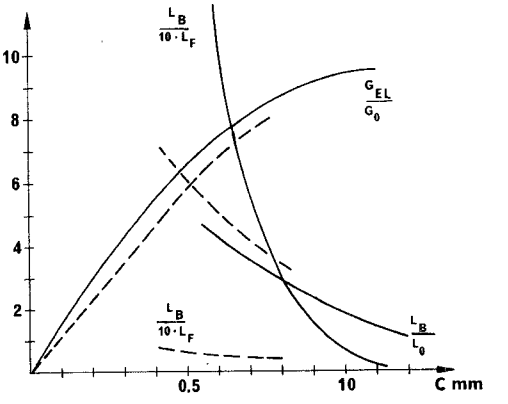

Fig. 8. Electronic gain (G_{el} dB), isolation (L_B dB), and forward wave attenuation in the isolator (L_F dB) at 22 GHz versus the cross-section dimensions of the waveguide maser (see Fig. 1). G_0 and L_0 are normalizing quantities. Full lines are for $A = 1.2$ mm and broken lines for $A = 0.8$ mm.

TABLE I

Maser type	Frequency range GHz	Total length mm	A mm	B mm	C mm	D mm
Dielectrically loaded waveguide	20-25	70	1.2	0.5	0.8	0.5
Dielectric image line	22-24.5	80	2.0	1.25	0.8	0.5
Dielectric image line	29-35	80	1.2	0.7	0.6	0.4

V. The Dielectric Image Line Maser

A dielectric image line supports a hybrid mode of the HE_{11} type (see, e.g., [12]). The structure has several advantages over the waveguide-type SWS described previously. Since only one crystal surface has to be in

intimate contact with the metal waveguide, one may solder the crystal to the waveguide surface. The chance of breaking the crystal is therefore almost eliminated. For soldering the crystal to the waveguide, the crystal had to be metallized and the titanium waveguide had to be gold plated. The metallization of the crystal was performed with an emulsion of silver and microscopic glass pearls (for adhesion) which were painted onto the surface and then heated at 700°C. The gold plating was done using ion plating and subsequent electroplating. The soldering was finally performed with an indium–tin solder (type 13 from the Indium Corporation of America).

A theoretical calculation of the $\omega - k$ diagram and the RF field configuration can be made using, e.g., the theory presented by Baier [12]. However, due to the high dielectric constants involved, a great number of terms in the field expansion are necessary, and the computing time becomes unacceptably long. Therefore, we have so far used an approximate approach. Consider a dielectric image line at the frequency ω where the guide wavelength is λ_g. The theoretical problem is now identical with the problem of calculating the resonance frequency of a dielectric resonator with "magnetic walls" at, say, $z = 0$ and $z = \lambda_g/2 \equiv \pi/k$. However, in the theory used for dielectric resonators [13], approximate magnetic walls are assumed not only at $z = 0$ and $z = \lambda_g/2$, but also at $y = \pm D$ (see Fig. 1). The resulting formula, then, relating ω to the length $\lambda_g/2 = \pi/k$ for a dielectric resonator with the cross-sectional dimensions C and $2D$ and confined in a waveguide of width A, becomes identical with (3) if one lets

$$k_w^2 \rightarrow k_D^2 + (\pi/2D)^2 \tag{4}$$

where k_w and k_D denotes the k values for the same ω for the waveguide structure and the dielectric image line structure, respectively. In fact, using (4) in (3) should give more accurate results for our case, where we do have "magnetic walls" at $z = 0$ and $z = \lambda_g/2$, than for the dielectric resonator case where calculated resonance frequencies are typically about 5 percent too low.

Hence comparing with the waveguide maser, we obtain for the dielectric image line maser

$$\omega_{cD} = \omega_w \left(k = \frac{\pi}{2D}\right) \tag{5}$$

$$k_D(\omega) = \sqrt{k_w^2(\omega) - \left(\frac{\pi}{2D}\right)^2} \tag{6}$$

$$S_D(\omega) = S_w(\omega)\sqrt{1 + \left(\frac{\pi}{2Dk_D}\right)^2} = \frac{S_w(\omega)}{\sqrt{1 - \left(\frac{\pi}{2Dk_w}\right)^2}}. \tag{7}$$

In Fig. 7 we show what happens when the waveguide maser is "transformed" into the mechanically less complicated and more reliable dielectric image line maser. With the same crystal size, the cutoff frequency is raised by as much as 100 percent. Measured slowing factors at room temperature and 25 GHz (corresponding to 22 GHz at 2 K) for the dielectric image line maser and the waveguide maser are 20 and 10, respectively.

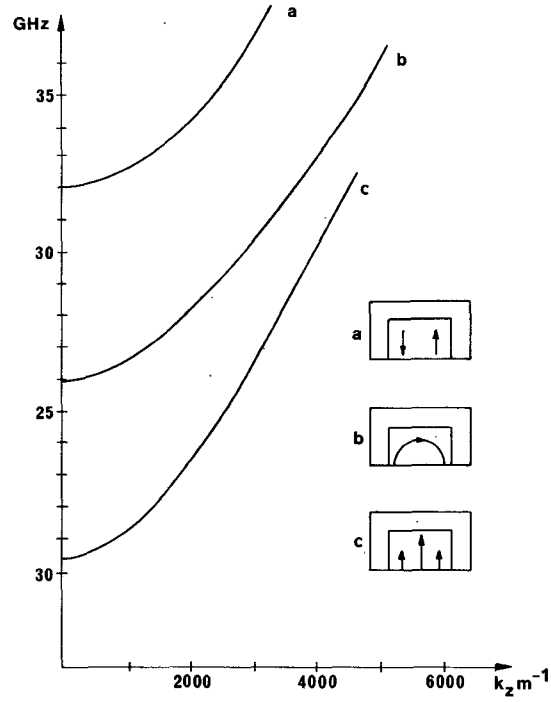

Fig. 9. Dispersion relations for the ground mode and the two lowest overmodes of the dielectric image line maser.

The exact solution for the $\omega - k$ diagram departs from the approximate dielectric resonator theory considerably at low k values. Hence a frequency band is obtained, where a backward wave does exist simultaneously with the forward wave. This phenomenon is predicted by more exact theories [12] and has also been observed in our measurements. Consequently, within about a 1-GHz frequency band ranging from the lowest observed transmission frequency, we get oscillations in the maser, and the isolation is much inferior here to that obtained at higher frequencies. This lack of isolation is consistent with the presence of a backward wave.

Another SWS property of importance is to determine when higher order modes will propagate. In Fig. 9 we depict the approximate $\omega - k$ diagrams of the lowest mode and the two higher order modes, as predicted by the dielectric resonator theory. Notice, however, that the symmetries of these two higher order modes will not allow coupling to the main mode or the input wave field unless irregularities in the structure are present. If energy is coupled into these modes, the isolator will work for both modes. Hence the overmode problem should not be serious until quite high frequencies are reached.

The theory predicts that the field energy will become more confined to the maser crystal and less to the isolator material as the frequency is increased. Consequently, the isolation will decrease with increasing frequency and will at some frequency become too small to prevent feedback

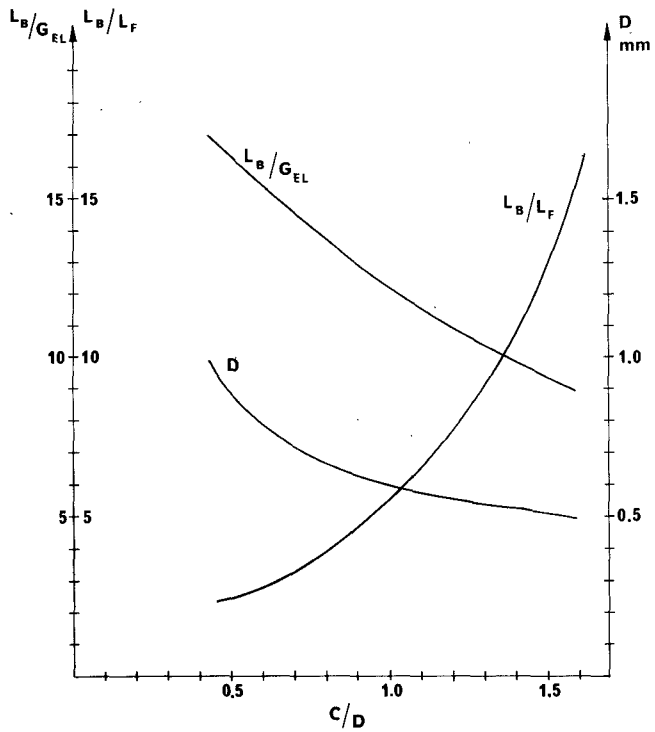

Fig. 10. Gain (G_{el}), isolator data (L_B and L_F), and the dimension D versus C/D at 22 GHz and $k_z = 3500\ m^{-1}$.

effects, which cause rapid frequency variations in the gain. This effect does in fact limit the tunable frequency range at the high end for both the waveguide maser and the dielectric image line maser. In Fig. 10 the ratio of isolator attenuation over electronic gain versus C/D as obtained from the dielectric resonator theory is shown. Lower values of C/D will not only increase the isolation–gain ratio, but will also enlarge the frequency gap between the HE_{11} mode and the first higher mode. In Table I the cross-sectional dimensions of the two dielectric image line masers are listed. Notice that C/D is smaller for the 30-GHz maser which also has the larger tunable bandwidth.

VI. Isolation of the Maser

Ferromagnetic resonance absorption is used for isolation of the amplifiers. The RF magnetic fields at the surface of the crystal (see Fig. 1) are to a large extent circularly polarized in the xz plane and the resonant attenuation of the reflected backward wave (L_B) will become much larger than the attenuation of the forward wave (L_F). In Figs. 8 and 10 the ratio L_B/L_F for the waveguide maser and the dielectric image line maser, respectively, is depicted. The resonance frequency of a piece of ferrite is determined by its geometry, by the intensity and direction of the applied magnetic field, and by the saturation magnetization of the ferrite [9]. Since the magnetic field and the ferrite geometry are already determined by the requirements of the crystal and the SWS, however, only the saturation magnetization M_s remains as a variable parameter. We may affect M_s in two ways, namely, by the choice of ferrite material and by the way of applying the ferrite to the crystal. The latter procedure will affect the density of the material and therefore also the effective M_s.

We have obtained good results using Trans Tech TT-111 material ($M_s = 7000$ Oe at 4.2 K), which we milled into a fine powder. A mixture of this powder and low-temperature varnish could easily be applied on the side of the crystal, yielding an M_s value of 2000 Oe at 4.2 K. Isolation of more than 80 dB (the limit in the measurements) over the frequency band 22–25 GHz could easily be obtained. However, since the electronic gain is almost the same in the forward as in the backward direction, the actual isolation is considerably larger than 80 dB in the lower part of the frequency band. The gain variations seen between 24 and 25 GHz [Fig. 2(b)] are mainly due to lack of complete isolation.

VII. Noise Considerations

Since 0.1-dB attenuation in the input room-temperature waveguide introduces a noise temperature of 7 K, one has to keep the input waveguide losses as small as possible. We have therefore designed a so-called "tall waveguide" [14], which is an oversized rectangular waveguide, in this case with the same cross-sectional dimensions as for an X-band waveguide ($a = 22.86$ mm, $b = 10.13$ mm), excited in the TE_{01} mode. The theoretical attenuation at 22 GHz of this waveguide is three times lower than in an ordinary K-band (18–26 GHz) waveguide. Moreover, the seven unwanted modes at 22 GHz can be filtered out with transverse slots in the broad side of the waveguide. This is essential, since higher order modes may be trapped, e.g., between tapers to the standard K-band waveguide size at the maser and at the feed horn, causing resonant absorption [14]. The mode filter is built into the tapered section at the cooled end of the waveguide in order to minimize the noise introduced by the filter. The tall waveguide consists of a standard stainless-steel X-band waveguide, with a thin layer ($\sim 1\ \mu m$) of gold electroplated onto the inner surface.

The noise temperature contribution of the maser package at the input waveguide flange was determined to be 27 ± 4 K using the sliding short technique [15] and verified with the hot–cold body technique. The noise contribution from the maser structure could be estimated by short circuiting the input waveguide close to the input terminal of the SWS. Hence the input waveguide contributes with 18 ± 2 K and the maser structure with 9 ± 2 K. More carefully manufactured waveguide and SWS's should enable us to decrease the losses and the noise temperature contributions somewhat. The measured maser structure noise temperature exceeds the theoretical one of 5 ± 1 K, as determined by the well-known formula for the noise temperature of the TWM as given by Siegman [9]. This discrepancy may be explained by a lower gain per unit length in the first part of the SWS, which may be partly due to the domain structure of the crystal (see Fig. 11) and partly due to the fact that the pump power is fed into the structure from the output waveguide part.

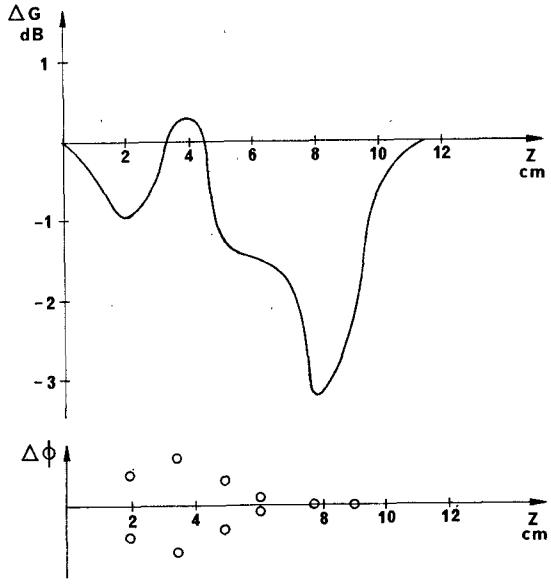

Fig. 11. Gain variations (ΔG dB) versus position along the 22-GHz maser in a magnetic-field-perturbation experiment and a schematic diagram showing the corresponding variations in axes orientations ($\Delta\phi$, arbitrary units) of single crystalline domains as observed in Laue-diffraction experiments. Notice that the largest change in gain is associated with a region where only one single crystalline domain is observed.

VIII. Pumping the Maser

Pumping of the maser was performed through the output K-band waveguide. The pumpwaves were simply injected into the signal waveguide through pump waveguides below cutoff for the signal frequency. A waffel-iron filter [16] at an optimized distance from the injection hole of the lower pump frequency improves the saturation of the maser and protects the mixer following the maser from being exposed to the pump power. A disadvantage with this injection method is that the injected pump power is to a large extent coupled into modes that do not couple very well to the maser crystal. For the 32-GHz maser we therefore injected the 70-GHz pump power using a K-band waveguide cross. The four arms were connected to 1) the maser, 2) a tunable short circuit, 3) a pump waveguide below cutoff for the signal frequency, and 4) the mixer receiver. Contrary to the 32-GHz signal, the 70-GHz pump power passes directly through the cross [arm 3) to 1)] with negligible coupling to the branching waveguides [2) and 4)]. The approximately 100 mW available was enough for a reasonable saturation of all three masers for all of which a 1-dB decrease in pump power yields a 1-dB decrease in gain. For the 32-GHz maser it was found difficult to saturate the whole paramagnetic resonance line, however, although the klystrons were frequency modulated, as for the 22-GHz masers. A more efficient pumping should therefore result in a broader bandwidth of the maser.

Since we measured a signal attenuation through the maser of about 10 dB, we decided to check the saturation of the pump transitions along the crystal. This was performed by moving a small iron ball along the crystal at the outside wall of the SWS. This iron ball created a small magnetic-field perturbation in the length interval ΔL of the crystal. The expected decrease of the maser gain in a completely saturated maser should be independent of the position (except at the ends of the crystal) and equal to $\alpha G_{el}\Delta L/L$, where $\alpha < 1$ is a constant depending on the detailed form of the field perturbation. A typical result of a perturbation measurement is shown in Fig. 11. By means of X-ray Laue diagrams we could completely understand the irregular form of the measured curve as due to single crystalline domains within the rutile crystal. Since virtually no difference could be seen comparing diagrams obtained with full pump power and with reduced pump power (−5 dB), one may conclude that each part of the crystal is equally saturated.

IX. The Maser Package

The complete maser also includes a dewar system for cooling and a superconducting magnet. The dewar has a capacity of about 15 l liquid helium, which is reduced to about 9 l when the temperature is decreased to 2 K by lowering the pressure to 30 torr. We expect the dewar to allow a total operating period of about three days on the telescope without refilling liquid helium.

The superconducting magnet is of the same type as that described by Hentley [17]. The field homogeneity is good enough not to noticeably broaden the absorption line more than the broadening obtained from the isolator material. Hence the field homogeneity is equal to or better than ±25 G at 6.5 kG required for the 22-GHz maser.

Acknowledgment

The authors wish to thank Prof. O. E. H. Rydbeck for his support during the project, C. O. Lindström for his able assistance and for performing many of the experiments, and A. Gustafsson for his excellent machine work and crystal grinding.

References

[1] B. E. Turner, "Interstellar molecules," *Scientific American*, vol. 228, no. 3, pp. 50–69, March 1973.
[2] E. L. Kollberg, "A traveling wave maser system for radio astronomy," *Proc. IEEE*, vol. 61, pp. 1323–1329, Sept. 1973.
[3] M. S. Reid, R. C. Clauss, D. A. Bathker, and C. T. Stelzried, "Low-noise microwave receiving systems in a world-wide network of large antennas," *Proc. IEEE*, vol. 61, pp. 1330–1335, Sept. 1973.
[4] V. I. Zagatin, G. S. Miserzhnikov, and V. B. Shteynshleyger, "Ruby maser operating in the 8 mm range," *Radio Eng. El. Phys.*, vol. 12, pp. 501–502, March 1967.
[5] F. Arams and B. Peyton, "Eight-millimeter traveling wave maser and maser radiometer system," *Proc. IEEE*, vol. 53, pp. 12–23, Jan. 1965.
[6] A. G. Cardiasmenos, K. S. Yngvesson, and E. L. Kollberg, "Maser amplifiers for the 20–24 GHz using ruby and iron-doped rutile," IEEE International Microwave Symposium, Boulder, CO, June 1973.
[7] C. Louis Cuccia, "Ultralow-noise parametric amplifiers in communication satellite earth terminals," *Advances in Microwaves*, vol. 7, 1973.
[8] A. G. Cardiasmenos, J. F. Shanley, and K. S. Yngvesson, "A traveling-wave maser amplifier for 85–90 GHz using a slot-fed image guide slow-wave circuit," this issue, pp. 725–730.
[9] A. E. Siegman, *Microwave Solid State Masers*. New York: McGraw-Hill, 1964.
[10] P. O. Anderson, E. L. Kollberg, and A. Jelenski, "Charge compensation in iron-doped rutile," *J. Phys. C.*, vol. 7, pp. 1868–1879, 1974.
[11] P. H. Vartanian, W. P. Ayres, and A. L. Helgesson, "Propagation in dielectric slab loaded rectangular waveguide," *IRE Trans. Microwave Theory Tech.*, vol. MTT-6, April 1958.

[12] W. Baier, "Waves and evanescent fields in rectangular waveguides filled with a transversely inhomogenous dielectric," *IEEE Trans. Microwave Theory Tech.*, vol. MTT-18, Oct. 1970.
[13] S. Nauman and J. S. Sethares, "Design of microwave dielectric resonators," *IEEE Trans. Microwave Theory Tech.*, vol. MTT-14, pp. 2–7, Jan. 1966.
[14] E. A. Benson, *Millimeter and Submillimeter Waves*. London: Iliffe Books Ltd., 1969.
[15] E. L. Kollberg, "On measurements of noise in low-noise receiving systems," *IEEE Trans. Instrumentation and Measurements*, vol. IM-23, pp. 226–232, Sept. 1974.
[16] G. L. Matthaei, L. Young, and E. M. T. Jones, *Microwave Filters, Impedance-Matching Networks, and Coupling Structures*. New York: McGraw-Hill, 1964.
[17] E. L. Hentley, "Superconducting magnet for an 8 mm travelling-wave maser," *Cryogenics*, vol. 7, pp. 33–35, Feb. 1967.

A Traveling-Wave Maser Amplifier for 85–90 GHz Using a Slot-Fed Image-Guide Slow-Wave Circuit

APOSTLE G. CARDIASMENOS, MEMBER, IEEE, JAMES F. SHANLEY, MEMBER, IEEE, AND K. SIGFRID YNGVESSON, MEMBER, IEEE

Abstract—**A description is given of a newly developed traveling-wave maser amplifier for use at the new 13.7-m millimeter-wave radio telescope of the Five College Radio Astronomy Observatory (FCRAO) near Amherst, MA. The maser amplifier, using iron-doped rutile as the active maser material, has achieved 15-dB electronic gain in the prototype over an instantaneous bandwidth of 140 MHz in the frequency range from 85 to 90 GHz. The use of a slot-fed image-guide mode which provides a wide-bandwidth coupling to the maser material is described and analyzed. Reduction of the total system noise temperature to less than 100 K including the atmosphere can be realized with these maser devices providing an order of magnitude improvement in system sensitivity.**

I. Introduction

In the past several years, interest among radioastronomy researchers to detect rotational transitions of polyatomic molecules in interstellar space has spurred development of low-noise millimeter-wavelength receiver systems. This paper describes the prototype design of a series of millimeter-wave maser amplifiers utilizing iron-doped rutile (Fe^{3+}–TiO_2) as the active maser material. These amplifiers will allow total system noise temperatures in the range 70–120 GHz, to approach the atmospheric noise limit. The initial maser developed for the frequency range 85–90 GHz will enable reduction of the total system noise temperature including the atmosphere to less than 100 K SSB. This should be compared to the 600–800 K SSB system temperatures achieved by the present lowest noise systems which use Schottky-barrier diode mixers.

Previous masers in this frequency range have all been single-port reflection cavity devices [1]–[4]. Cavity masers are limited to a fairly narrow instantaneous bandwidth and are also, along with other reflection-type negative resistance amplifiers, not sufficiently stable at gains above about 15 dB. These amplifiers also require the development of low-noise cooled circulators operable at millimeter wavelengths. Typical cavity maser bandwidths of less than 20 MHz may be expected in this frequency range, while interstellar molecular spectral lines many times have linewidths exceeding 50 MHz. The instantaneous bandwidth of a traveling-wave maser, however, can be approximated by the relation [5]

$$\Delta f = \Delta f_L \left[\frac{3}{G_{\mathrm{dB}}{}^{e} - 3}\right]^{1/2} \tag{1}$$

where Δf_L is the intrinsic paramagnetic absorption linewidth, and $G_{\mathrm{dB}}{}^{e}$ is the midband maser electronic gain. For a typical electronic gain of 30 dB, and $\Delta f_L = 300$ MHz (measured in iron-doped rutile at 85 GHz), an instantaneous bandwidth of 100 MHz results, which is well suited to investigation of interstellar spectral lines. The electronic gain is given by [5]

$$G_{\mathrm{dB}}{}^{e} = 27.3 \cdot S \cdot \frac{1}{|Q_m|} \cdot \frac{L}{\lambda_0}. \tag{2}$$

Here S = the slowing factor = c/v_g where c is the speed of light in vacuum and v_g is the group velocity with which the wave propagates through the maser structure, L is the length of active material from input to output, λ_0 = the free-space wavelength at the signal frequency, and Q_m is the magnetic quality factor of the maser material. In order to develop a useful traveling-wave millimeter-wave maser,

Manuscript received December 29, 1975; revised May 4, 1976. This work was supported by the National Science Foundation under Grants GP 26108, GP 38593X, and MPS75-09730. This paper is contribution number 227 of the Five College Radio Astronomy Observatory.

A. G. Cardiasmenos is with the Department of Physics and Astronomy and the Five College Radio Astronomy Observatory, University of Massachusetts, Amherst, MA 01002.
J. F. Shanley and K. S. Yngvesson are with the Department of Electrical and Computer Engineering and the Five College Radio Astronomy Observatory, University of Massachusetts, Amherst, MA 01002.